ADVANCED MATERIALS
www.advmat.de

Degeneracy Removal of Spin Bands in Collinear Antiferromagnets with Non-Interconvertible Spin-Structure Motif Pair

*Lin-Ding Yuan and Alex Zunger**

Energy bands in antiferromagnets are supposed to be spin degenerate in the absence of spin–orbit coupling (SOC). Recent studies have identified formal symmetry conditions for antiferromagnetic crystals in which this degeneracy can be lifted, spin splitting,even in the vanishing SOC (i.e., non-relativistic) limit. Materials having such symmetries could enable spin-split antiferromagnetic spintronics without the burden of using heavy-atom compounds. However, the symmetry conditions that involve spin and magnetic symmetry are not always effective as practical material selection filters. Furthermore, these symmetry conditions do not readily disclose trends in the magnitude and momentum dependence of the spin-splitting energy. Here, it is shown that the formal symmetry conditions enabling spin-split antiferromagnets can be interpreted in terms of local motif pairs, such as octahedra or tetrahedra, each carrying opposite magnetic moments. Collinear antiferromagnets with such a spin-structure motif pair, whose components interconvert by neither translation nor spatial inversion, will show spin splitting. Such a real-space motif-based approach enables an easy way to identify and design materials (illustrated in real example materials) having spin splitting without the need for SOC, and offers insights into the momentum dependence and magnitude of the spin splitting.

1. Introduction

The interplay between physical interactions and the systems' symmetry constitute the law of nature. For example, the relativistic spin–orbit interaction term in the presence of inversion asymmetry in nonmagnetic crystals results in the splitting of spin-polarized energy bands (henceforth "spin spitting") known as Rashba[1] and Dresselhaus[2] effects. Likewise, the interaction between electron spin and spontaneous inhomogeneous magnetic field in antiferromagnets was anticipated in 1964 by Pekar and Rashba[3] to result in an unusual momentum-dependent spin splitting that does not rely on SOC. Yet, many common antiferromagnetic crystals, such as NiO and MnO, do not show such spin splitting. This begs the question of what the symmetry conditions are enabling such a mechanism. More generally, the obvious need to validate experimentally novel proposed mechanisms calls for establishing the symmetry conditions needed for identifying candidate real materials that could harbor such effects. In collaboration with Wang, Luo, and E. Rashba, the present authors have recently formulated the enabling symmetry conditions for SOC-independent spin splitting[4] Such symmetry conditions disentangle the SOC-independent splitting from the SOC-induced splitting by considering the symmetry at the zero SOC limit (i.e., spin symmetry,[5] where spin and space are fully decoupled). Analysis based on the spin symmetry alone was later presented by Smejkal et al.[6] Despite being rigorous, the symmetry theory[4,6] did not amount to a transparent structural chemistry intuition for the enabling principles and could not be used to predict the magnitude and momentum-dependence of the spin splitting. The alternative model Hamiltonian-based approach[7] also does not provide a straightforward way to identify materials that harbor spin splitting without SOC. The difficulty for a crystal chemist to look at the rule of simultaneous violation of the symmetry conditions and suggest predictively a specific real compound following this violation would appear to impede experimental developments in this field. Indeed, designed experimental efforts in this field are only known for a few limited systems, such as RuO_2.[8]

This difficulty can be eased by bridging the spin symmetry rule and the crystallographic structural motifs[9]—a common practice used in solid state chemistry and crystallography to assert the crystal structures. Intriguingly, the bridge is implied by and linked to some fundamental facts of the spin-splitting effect in antiferromagnet: 1) The traditional picture of magnetism—magnetic moments anchored on magnetic atomic sites (see **Figure 1**a)—cannot explain why antiferromagnet with zero net magnetization would have spin splitting. 2) Considering the spontaneous magnetization as spatially inhomogeneous allows one to anticipate spin splitting.[3] Mathematically, the real space distributed inhomogeneous magnetization can be expanded into

L.-D. Yuan, A. Zunger
Renewable and Sustainable Energy Institute
University of Colorado Boulder
Boulder, CO 80309, USA
E-mail: alex.zunger@colorado.edu

The ORCID identification number(s) for the author(s) of this article can be found under https://doi.org/10.1002/adma.202211966

DOI: 10.1002/adma.202211966

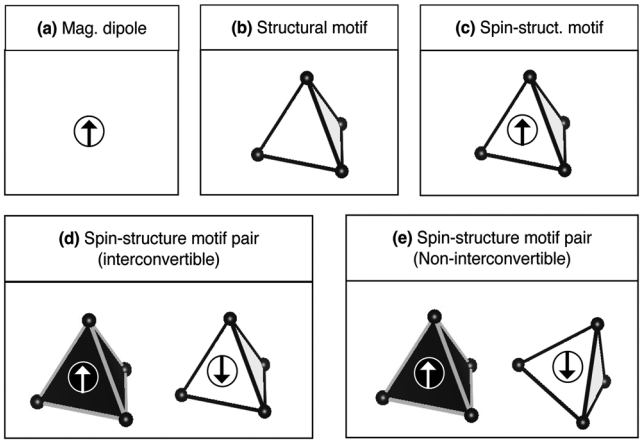

Figure 1. Antiferromagnets with interconvertible/non-interconvertible spin-structure motif pair. a) magnetic moment anchored on individual magnetic atomic sites; b) structural motif that defines the local chemical and coordination environment and is the building block of a crystal; c) spin-structure motif that conjugates magnetic moment and the structural motif; d) spin-structure motif pair that interconverts by inversion and/or translational e) spin-structure motif pair that cannot interconvert by inversion nor translation. The tetrahedra with circled spin inside are used to represent the spin-structure motifs; a black and a white tetrahedron associated with the spin-structure motif of magnetic moment pointing up and down forms a spin-structure motif pair. The orientation of the magnetic moments is indicated by the color of the tetragonal and the direction of the arrows within the circle.

magnetic dipole term and magnetic multipole terms.[10] Recently, magnetic octupole order[11] was used to describe the unconventional SOC-independent spin-splitting effects in antiferromagnets. 3) In real magnetic crystals, magnetic atoms are usually embedded in some local structural motifs formed by non-magnetic atoms. The geometry of the structural motif—such as tetrahedra (see Figure 1b) in zinc-blende crystals, or octahedra in perovskite crystals—largely defines the shape of the localized d or f orbitals and therefore the geometry of the local magnetization that "lives" within the motif. This echoes the demonstrated decisive role nonmagnetic atoms play[12] in determining the spin splitting behavior in different antiferromagnets. Recognizing magnetism as arrays of geometric objects that carry concomitant magnetic moments adapts these facts.

Here, we introduce the generalized structural motif combined with magnetic moments, referred to here as a spin-structure motif (see Figure 1c). Collinear antiferromagnets have two flavors of such spin-structure motifs—motifs carrying "up" magnetic moment and motifs carrying "down" magnetic moment—which form the "spin-structure motif pair". The enabling symmetry conditions can then be interpreted in terms of the geometric relation, interconvertible or non-interconvertible, between the two flavors of the spin-structure motifs. Antiferromagnets comprises of interconvertible (non-interconvertible) spin-structure motif pair—motifs of one flavor are mutually related (unrelated) to the other flavor by certain spatial transformation—preserves (violates) the symmetry conditions for spin-degeneracy. Such a motif-based rule thus allows discerning spin-split antiferromagnets (referred to as SST-4 antiferromagnets in ref. [4]) from spin-degenerate antiferromagnets (referred to as SST-1, SST-2, or SST-3 antiferromagnets in ref.[4]). We illustrate the rule on real compounds and validated it by density functional calculations. We also discussed insights on the momentum dependence and magnitude of the spin splitting that is beyond what symmetry analysis[4] could offer.

2. The Motif-Based Rule

2.1. The Enabling Symmetry Conditions for SOC-Independent Spin Splitting in Antiferromagnets

We first summarize the enabling symmetry conditions derived in ref. [4] for the SOC-independent spin splitting. This considers the symmetry at the zero SOC limit,[5] where spin and space are fully decoupled. The pertinent individual symmetry operations are: U being a spin rotation of the SU (2) group acting on the spin 1/2 space that reverses the spin; T being spatial translation; Θ being time reversal, and I being the spatial inversion. These individual operations are then used for constructing two symmetry products: a SOC-free magnetic symmetry ΘIT, and a spin symmetry UT (where the former product can be simplified to ΘI by proper choice of inversion center). SOC-independent spin splitting would occur only when both symmetry products are simultaneously violated. The two symmetry products were then mapped into magnetic space group symmetries[13] (that in the most general form include time reversal and consider SOC), thereby allowing the use of the tabulated magnetic structure symmetry information provided in the material database[14] to sort out candidate materials.[4b] Such mapping is further discussed in Supporting Information Section A, which justifies the use of magnetic space group symmetry to describe the spin effect without SOC.

2.2. Spin-Structure Motif as a Descriptor of the Symmetry

Because the symmetry operation U and Θ reverses the collinear magnetic ordering, the preserving (violation) of UT symmetry in a collinear antiferromagnetic compound corresponds to the spin-structure motifs of one flavor can (cannot) be interconverted to motifs of the other flavor by a non-primitive translation T of the magnetic unit cell. Similarly, the preservation (violation) of ΘI symmetry means the spin-structure motifs of one flavor can (cannot) be interconverted to motifs of the other flavor by spatial inversion.

Considering the simplest case where the collinear antiferromagnet has a pair of spin-structure motifs in the magnetic unit cell. As illustrated in Figure 1d, the two tetrahedra, each carrying a magnetic moment but anti-aligned, form a spin-structure motif pair. The two tetrahedra related by a translation (which could also be an inversion) are interconvertible. Antiferromagnets of this prototype will not show spin splitting without SOC; In contrast, as illustrated in Figure 1e, the two tetrahedra are neither related by a translation nor inversion, therefore form a non-interconvertible spin-structure motif pair. Antiferromagnets of this prototype will show spin splitting without SOC. Further division of the two prototypes based on whether the spin-structure motifs are centrosymmetric or non-centrosymmetric is discussed in Supporting Information section B.

The same correspondence applies to collinear antiferromagnetic compounds with multiple pairs of spin-structure motifs in the magnetic unit cell. In this case, there are a group of (more than one) spin-structure motifs of the same flavor within the magnetic unit cell. The interconvertible relation shall be examined for a pair of such spin-structure motif groups of opposite magnetic moment. As such, collinear antiferromagnetic compounds with interconvertible spin-structure motif pair, whose component two groups are related by translation or inversion, will not exhibit spin splitting without SOC; collinear antiferromagnetic compounds with non-interconvertible spin-structure motif pair, whose component two groups are not related by translation nor inversion, will expect to show the SOC-independent spin splitting.

This connection between the spin-structure motif pair and the symmetry-enabled spin splitting derived from symmetry is general. It fails only when there exist additional non-magnetic atoms (not included in the spin motif pair) that lower the symmetry of the antiferromagnetic compounds. Because these additional atoms are not the nearest neighbors to the magnetic atoms, they have much less impact on the magnetization, and will only contribute to a negligible second-order spin splitting effect, we will ignore their effect.

2.3. Applying the Motif-Based Rule to Select Materials

The connection between non-interconvertible spin-structure motif pair and the breaking of the effect enabling symmetries readily provides a convenient guide for selecting candidate materials. The material selecting procedures are:

1) Start from a solid-state material of interest;
2) Identify the magnetic phase and magnetic configuration of the material, and proceed to step 3 only if the material becomes antiferromagnetic under a certain temperature;
3) Identify the crystal structure and its constituent structural motifs in the antiferromagentic phase;
4) Identify the spin-structure motifs in the magnetic unit cell;
5) Determine if the spin-structure motifs form interconvertible pair related by translation or inversion;
6) Determine if the material will exhibit spin splitting based on the answer to step 5.

The key to applying the procedures is to decide the spin-structure motifs of a material, i.e., step 3 and step 4. For those materials with known structure types, their structural motifs can be learned directly from the International Union of Crystallography (IUCr). For those materials with complex structures, their structural motifs can be determined via a Voronoï approach[15] based procedure.[16] This can be done automatically using the computational tool "pymatgen".[16] Further, by separating the structural motifs conjugated with up and down magnetic moments and limiting our focus to the magnetic unit cell, we can then get the spin-structural motif pair. Once the spin-structure motif pair is identified, the determination of the interconvertible relation between the spin-structure motif pair (step 5) is often obvious and so does the determination of the material (step 6). To show the predictive power of this methodology, we will illustrate it in a few selected real antiferromagnetic materials, but performing high-throughput screening of materials following the procedures is not the focus of this work and will leave for future exercise.

3. Illustration of the Motif-Based Rule in Real Materials

3.1. Antiferromagnets with a Pair of Spin-Structure Motifs

We will start from the simplest cases where there is only a pair of spin-structure motifs in the magnetic unit cell. **Figure 2**a shows the crystal structure of antiferromagnetic tetragonal CuMnAs,[17] in which the non-centrosymmetric $MnAs_5$ square-pyramid is alternatively aligned along the [001] direction. The two neighboring $MnAs_5$ square pyramids with opposite local magnetic moments constitute the spin-structure motif pair whose components interconvert by inversion but not translation. Similarly, antiferromagnetic trigonal $FeBr_2$[18] and hexagonal $BiCoO_3$,[19] as shown in Figure 2b,c respectively, contain a spin-structure motif pair whose components interconvert by inversion and/or translation. These three antiferromagnets belong to the interconvertible prototype illustrated in Figure 1d and will not show spin splitting. Interestingly, for $BiCoO_3$, the spin splitting is expected to be zero only when SOC vanishes. Theoretical studies [20] show finite spin splitting in this compound when SOC is considered—a case of SOC-induced splitting. In contrast to CuMnAs, $FeBr_2$, and $BiCoO_3$, antiferromagnetic rutile NiF_2,[21] shown in Figure 2d, contains a pair of differently oriented NiF_6 spin-structure motifs that are interconverted by neither translation nor inversion (instead related by a 90-degree in-plane rotation). This compound belongs to the non-interconvertible prototype illustrated in Figure 1c and will show the SOC-independent spin splitting. Isostructural antiferromagnets, such as MnF_2,[4a] RuO_2,[12b,22] and CoF_2,[4b,23] reported to show SOC-independent spin splitting, also contains a similar non-interconvertible spin-structure motif pair. DFT results of these representative example materials are shown in Figure S3 (Supporting Information), which agree well with the symmetry and motif description.

3.2. Antiferromagnets with Multiple Pairs of Spin-Structure Motifs

While the materials discussed in Section 3.1 are simple examples for the illustration of the motif-based rule, more common cases people dealing with are materials with multiple pairs of spin-structure motifs in the magnetic unit cell. We now discuss this general scenario.

The upper panel of **Figure 3**a shows the crystal structure of antiferromagnetic tetragonal $LaMn_2Si_2$.[24] It comprises two layers of edge-sharing non-centrosymmetric $MnSi_4$ tetrahedrons stacking along the *c*-axis. Within each layer, the $MnSi_4$ tetrahedra carry magnetic moments that are alternatively aligned, forming an in-plane antiferromagnetic ordering. The tetrahedra in the upper and the lower layers carrying opposite magnetic moments together constitute the spin-structure motif pair. Foregoing analysis shows (see lower panel of Figure 3a) the tetrahedra motif pairs are interconvertible by an inversion that connects the white

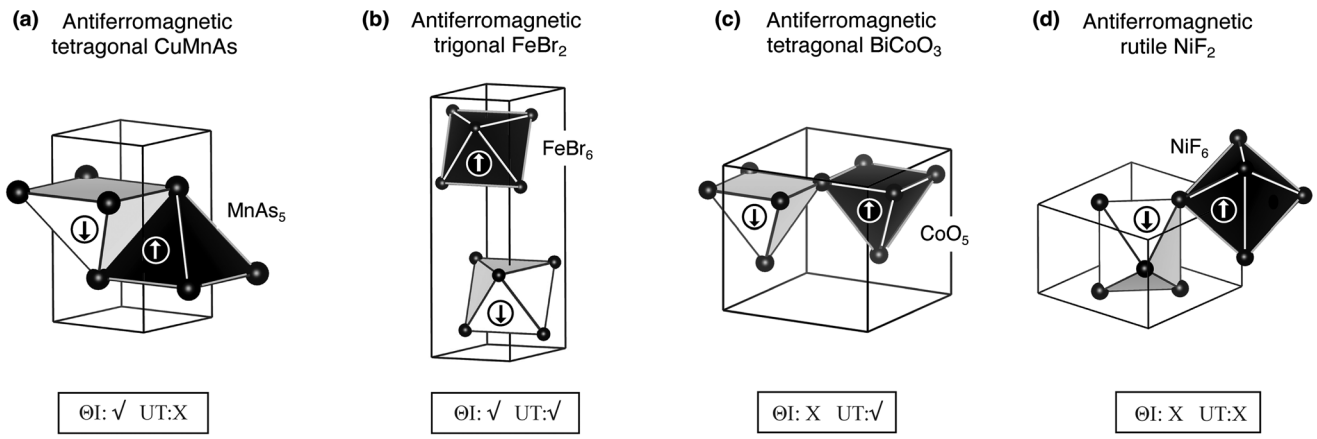

Figure 2. Examples of collinear antiferromagnetic compounds with a pair of spin-structure motifs. a) Tetragonal CuMnAs with spin-structure motif pair whose components interconvert by inversion. b) Trigonal $FeBr_2$ with spin-structure motif pair whose components interconvert by inversion and translation. c) Tetragonal $BiCoO_3$ spin-structure motif pair whose components interconverts by translation. d) Rutile NiF_2 with spin-structure motif pair whose components fails to interconnect by inversion and translation. Black and white colors are used to map the spin-structure motif pair with opposite magnetic moments. Periodically repeated spin-structure motifs within the same magnetic unit cell are removed to simplify the illustration.

tetrahedra to the black tetrahedra. This material in its antiferromagnetic phase thus belongs to the interconvertible prototype illustrated in Figure 1d and will not show spin splitting. Isostructural material $LaMn_2Ge_2$[24] also belongs to this prototype.

The upper panel of Figure 3b shows the crystal structure of antiferromagnetic orthorhombic $LaMnO_3$. It consists of eight corner-sharing MnO_6 octahedrons in the magnetic unit cell, which are ferromagnetically aligned in the *ac* plane and alternatively stacked along the *b*-axis. The four octahedra in the upper layer and four octahedra in the lower layer thus constitute the spin-structure motif pair. The octahedra are cooperatively tilted forming a pattern noted as $a^-b^+a^-$ following Glazer's notation.[25] This pattern comprises one in-phase ("+") rotation about the *b*-axis, and two out-of-phase ("−") tilts around *a*- and *c*-axes by the same angle. As a result, the octahedra are differently oriented which lowers the symmetry. Since the rotation or tilting angles are the same for all eight octahedra, their orientations can be uniquely described by the axis each octahedron rotates about. Foregoing analysis shows (see Figure 3b lower panel), the upper layer octahedra are "+++" and "−−−" oriented, while the lower layer octahedra are "−+−" and "+−+" oriented. Therefore, the two spin-structure motif groups of different flavors are not interconvertible by inversion or translation. For more details on how the orientation axis is derived for each octahedron, please refer to ref. [25]. This material in its antiferromagnetic phase thus belongs to the non-interconvertible prototype illustrated in Figure 1e and will show spin splitting. Isostructural materials, such as $PrMnO_3$,[26] and $NdMnO_3$,[27] belong to the same prototype.

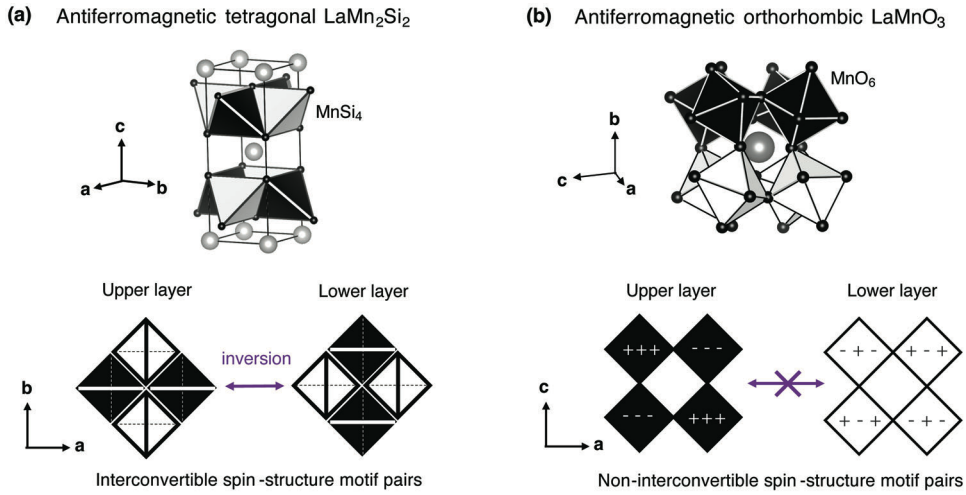

Figure 3. Examples of collinear antiferromagnets with multiple pairs of spin-structure motifs. a) Tetragonal $LaMn_2Si_2$ with interconvertible spin-structure motif pair. b) Orthorhombic $LaMnO_3$ with non-interconvertible spin-structure motif pair. In the lower panel of (b), the orientation of each octahedron is described by the axis (3 consecutive +/−) about which it rotates. Black and white colors are used to map the spin-structure motifs of the opposite magnetic moment.

4. Understand the Spin Splitting in Antiferromagnets from the Spin-Structure Motifs

Besides being a descriptor of the symmetry rules, the motif-based description also offers insights into the physics underpinning: what is the origin of the momentum-dependent spin splitting, and how will the symmetry-breaking affect the magnitude of the spin splitting. We will illustrate these points using the two non-interconvertible example compounds, rutile NiF_2 and orthorhombic $LaMnO_3$.

4.1. The Origin of the Momentum-Dependent Spin Splitting in Collinear Antiferromagnets

One of the mysteries the symmetry did not tell us is how momentum-dependent spin splitting arises from compensated magnetization. Viewing the spin structure motif pair from different perspectives offers insight. Let's look again at the non-interconvertible example material rutile NiF_2. As shown in **Figure 4**, by projecting the two NiF_6 spin-structure motifs in the magnetic unit cell onto the different real space crystallographic planes, we see that the difference in shapes emerges when the spin-structure motif pair is projected onto (110) planes but disappears when viewed from (100) perspective. This exactly maps to the k directions where the energy bands spin split (along [110] directions) and spin degenerate (along [100]). The correspondence can be understood as follows. When the projected spin-structure motif pair have the same shape, the "projected" magnetization is compensated, which ensures spin degenerate bands alone corresponding k direction. When the projected spin-structure motif pair have a different shape, the "projected" magnetization is uncompensated, which results in spin-split bands along corresponding k direction. Such correspondence between the "same versus different" shape of the two projected spin-structure motifs and "degenerate versus split" energy bands not only explains the emergence of the momentum-dependent spin splitting. But also provide an intuitive method to acquire information about at which momentum the spin splitting would occur, which otherwise requires sophisticated knowledge of the symmetries (beyond ΘI and UT) about the system[6] to figure out.

4.2. Spin-Structure Motif Pair and the Magnitude of the Spin Splitting

Another mystery that symmetry did not tell us is where the symmetry breaking comes from and how it is related to the magnitude of the spin splitting. Take lanthanoid perovskite manganite $LaMnO_3$ as an example. We discussed in Section 3.2 that the cooperative octahedral tilting breaks the symmetry, but it is not clear as yet how individual tilt contributes to the overall spin splitting effect and how the degree of the tilting angles affects the magnitude of the spin splitting. **Figure 5** shows the DFT calculated spin splitting (averaged spin splitting over occupied Mn e_g bands and a dense k-mesh, see method section for details) for different structural configurations of in-phase and out-of-phase tilt angles. As shown in Figure 5, decomposed individual in-phase or out-of-phase tilt modes ($\alpha = \gamma = 0$, $\beta \neq 0$) and ($\alpha = \gamma \neq 0$, $\beta = 0$) have no spin splitting; while the composite cooperative tilt modes ($\alpha = \gamma \neq 0$, $\beta \neq 0$) have finite spin splitting. The magnitude of the spin splitting increases as the tilting angles become larger. Small randomness observed in the heatmap may be attributed to the unavoidable octahedral distortions accompanied by tilting. Further quantitative analysis suggests the curved shape of the resulting spin splitting Δ_{SS} can be approximately fitted to the product of the tilting angle about the a and c axes (α or γ) and the tilting angle about the b-axis (β), that $\Delta_{SS} \approx 0.3\alpha\beta$ (meV). Since octahedral tilting can be controlled via common engineering methods, such as epitaxial strain,[28] interface engineering,[29] or strain doping,[30] fitted equations like this will be very useful in predicting and designing perovskite materials having a sizable spin splitting effect.

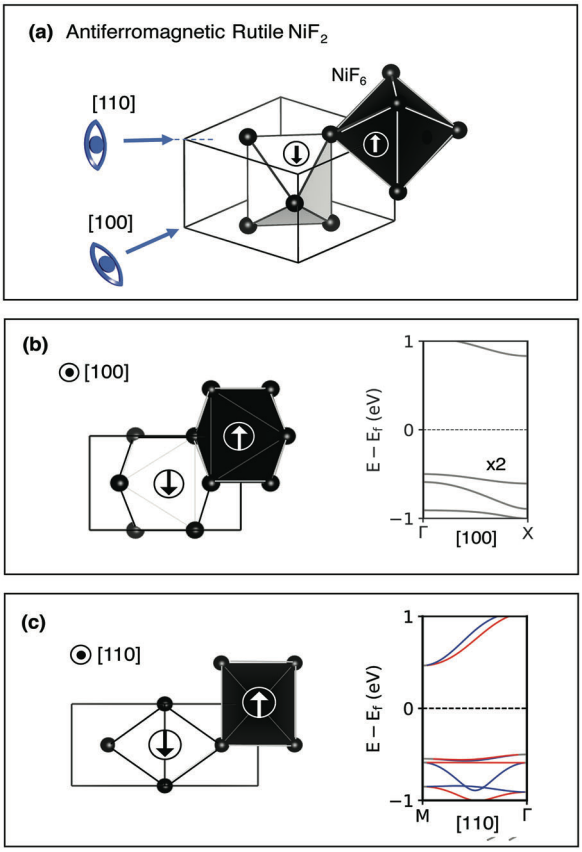

Figure 4. The relation between spin-structure motif pair and the momentum-dependent spin splitting. a) The crystal structure of rutile NiF_2 constitutes a non-interconvertible spin-structure motif pair—black and white octahedrons. b) The [100] perspective of the spin-structure motif pair. c) The [110] perspective of the spin-structure motif pair. Solid dots are used to represent F atoms coordinated around Ni atoms. The red and blue lines depict the positive and negatively spin polarized bands. The gray lines are spin degenerate bands with no spin polarization.

Besides the tilting angles, the magnetic ordering also has an impact on the resulting spin splitting in $LaMnO_3$. **Figure 6** compares the spin splitting effect for assumed C-type, E-type, and G-type antiferromagnetic ordering, where the spin splitting behavior is contrastingly different. When the $LaMnO_3$ takes the C-type antiferromagnetic ordering, the material has

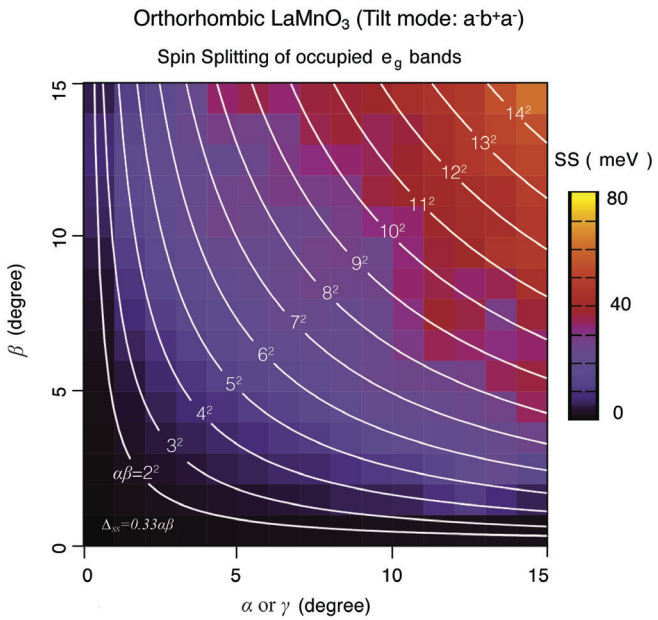

Figure 5. Dependence of the magnitude of spin splitting in antiferromagnetic orthorhombic $LaMnO_3$ on the octahedral tilting angles. The magnitude of the spin splitting is evaluated as an average over occupied Mn e_g bands which is right below the fermi level. The amplitude of the spin splitting ranges from 0 to 80 meV and is mapped to continuous color change from dark purple to light yellow. The white auxiliary lines inside the heatmap are a set of $\alpha\beta$ = constant curves.

interconvertible spin-structure motif pair, and the spin splitting is zero. When the antiferromagnetic ordering is E-type or G-type, the material has non-interconvertible spin structure motif pair, and the spin splitting is finite. The last column of Figure 6 lists the magnitude of the spin splitting of the occupied eg bands, we see the C-type has zero spin splitting, the E-type has a value of 40.4 meV, and the G-type has the largest splitting of 74.4 meV. This increasing trend from C-type to E-type to G-type reflects the growing degree of symmetry breaking which is indicated by the number of non-interconvertible motif pairs (going from 0 to 2 to 4).

More specifically, for C-type antiferromagnetic ordering, the black and white spin-structure motif group contains the same set of oriented octahedra—that is one "+++", one "−−−", one "+−+", and one "−+−" oriented octahedron. Therefore, each tilted black octahedron has a corresponding white octahedron with the same tilting, together they form an interconvertible spin-structure motif pair. In total, that is four interconvertible spin-structure motif pairs and zero non-interconvertible spin-structure motif pairs. Meanwhile for E-type and G-type antiferromagnetic ordering, as illustrated in Figure 6 second and third columns, the number of non-interconvertible spin-structure motif pairs is two and four, respectively. It is clear that the larger the number of non-interconvertible motif pairs the larger the degree of symmetry breaking, and the spin splitting. For materials with multiple spin-structure motif pairs, the number of non-interconvertible motif pairs is thus a good indicator of the magnitude of the spin splitting.

5. Discussion

Here, we briefly explore the potential broader impact of the ideas developed in the current paper into a few other domains. We note that looking at the spin splitting effect as a consequence of the individual spin-structure motifs failing to mutually interconvert or not only offers a way to tell if an antiferromagnetic compound will enable us to see whether symmetries are preserved or violated; but also helps to find the future connection to other functionalities (such as, bonding and stability) that are traditionally expressed by structural motifs.

5.1. Spin Splitting in Noncollinear Antiferromagnets

While the current paper focuses on the discussion of collinear antiferromagnetic compounds, we note that the SOC-independent spin splitting effect can also exist in noncollinear antiferromagnetic compounds. The application of the motif-based method on noncollinear antiferromagnets is similar to that in collinear antiferromagnets but the spin-structure motif is no longer limited to two flavors of "black" and "white". Thus, the interconvertible relation should be checked for each set of spin-structure motifs whose magnetic moments are aligned in the same direction (parallel or antiparallel). For example, the $ThCr_2Si_2$-type antiferromagnetic KMn_2S_2 (shown in Figure S3, Supporting Information), has an alternate noncollinear magnetic ordering[31] aligned along the [110] and the [1−10] directions. The spin-structure motifs of this material can then be separated into two sets—one contains magnetic moments that are [110] aligned, the other contains magnetic moments that are [1−10] aligned. Since both sets of the spin-structure motif pairs are related by the same inversion, the material thus belongs to the interconvertible prototype, lacking spin splitting. Additionally, one should note that the symmetry condition of preserving UT in coplanar noncollinear antiferromagnets does not always guarantee spin degeneracy. When the spin states are not aligned in the same plane of the coplanar plane, the *UT* symmetry may not reverse the spin states as it does in the collinear magnetic systems.

5.2. Antiferroelectric Material with Non-Interconvertible Electric-Structure Motif Pair

Analogous to the spin-structure motif one can define a structural motif carrying an electric dipole as an electric-structure motif. Antiferroelectric materials can then be described by electric-structure motif pair, whose components carry opposite electric dipoles that compensate. This discerns Antiferroelectric materials with electric-structure motifs that are interconvertible and non-interconvertible. Novel properties might emerge in the latter prototype. Moreover, multiferroic ordering arises when the structure motif is entangled with both magnetic dipole and electric dipole. A comprehensive motif-based description of the coupled orders—magnetic order, electric order, and structure motif order—may be beneficial for the study of the encoded multiferroic ordering. Particularly, one possibility would be antiferroelectric antiferromagnets with non-interconvertible spin-structure motif pair and non-interconvertible electric-structure motif pair.

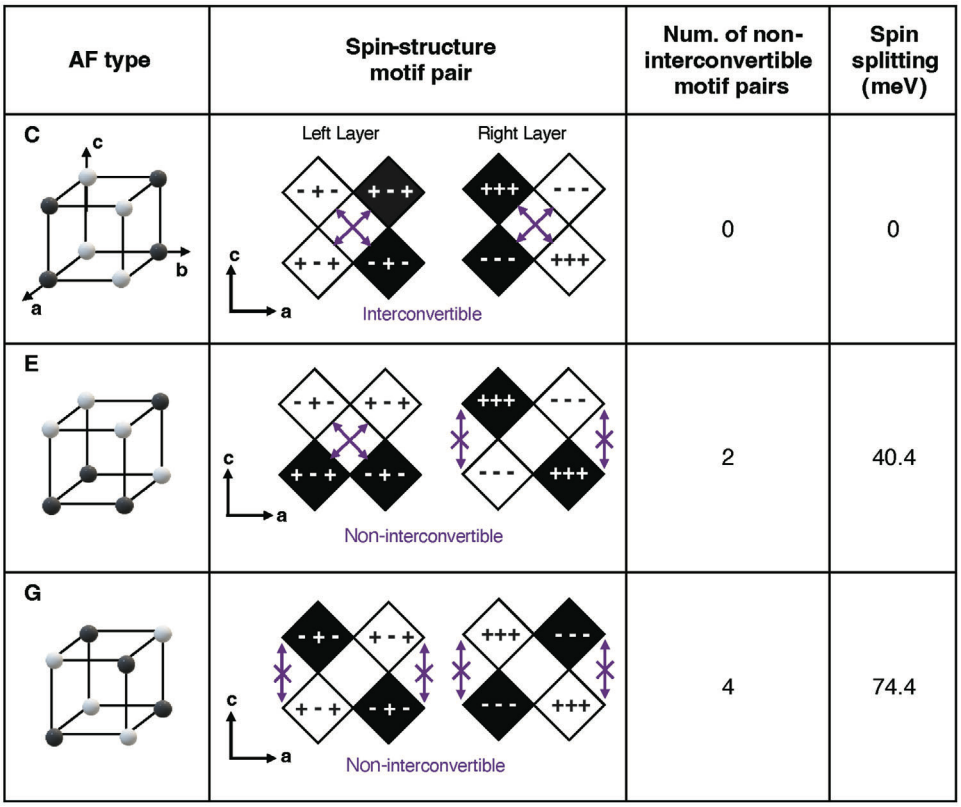

Figure 6. Dependence of the magnitude of spin splitting in antiferromagnetic orthorhombic $LaMnO_3$ on‘ antiferromagnetic type. Black and white colors are used to map the two flavors of the spin-structure motifs carrying opposite magnetic moments. The purple arrows (with a cross) in between the black and white shapes are used to indicate the interconvertible (non-interconvertible) relation between the motifs. The spin splitting is evaluated as the averaged value of the occupied Mn e_g bands.

5.3. Design of Multifunctional Materials

The motif language highlighting how atoms see each other in the local coordination environment is closely associated with many material properties. For example, the tetrahedral versus octahedral coordination of Mn^{2+} ions are associated with the formation or absence of polarons which limits electric conductivity.[32] The tetrahedral coordination associated with the sp^3 hybridization determines the electronic and optical properties of many zinc-blend semiconductors.[33] Recently, the structural motif descriptor has also been applied in machine learning studies to predict the electronic properties of materials.[34]

Combining other functionalities with the emergent spin splitting in antiferromagnets with non-interconvertible spin-structure motif pair would facilitate the design of new multifunctional materials.[9a,b,35] A particularly interesting combination is spin-split antiferromagnet in the presence of ferroelectricity/antiferroelectricity. In the spin-split antiferromagnet $LaMnO_3$, ferroelectricity can be introduced by replacing the A-cation La^{3+} with Tl^+, Pb^{2+}, or Bi^{3+} with $6s^2$ lone pair electrons. Indeed, $BiMnO_3$ was reported to have a ferroelectric distortion[36] (associated with a dynamically unstable phonon mode at Γ). However, $BiMnO_3$ takes ferromagnetic ordering. Other Bi-based perovskites, such as $BiCrO_3$ with G-type antiferromagnetic ordering under 123K,[37] may be candidates. Another interesting combination to contemplate is spin-split antiferromagnet and half-metallicity[38] (i.e., metallic in one spin direction and semiconducting in the other). The traditional design scheme for the half-metallic antiferromagnet is to include different magnetic ions with the same moment that are anti-aligned. Antiferromagnets fulfilling the conditions are rare. A potential new scheme suggested here is to design antiferromagnets with the same magnetic ions with magnetic moment anti-aligned but are in different local structural coordination environments. The latter arrangement is exactly what we meant by antiferromagnets with non-interconvertible spin-structure motif pair, where the component spin-structure motifs cannot be mutually interconverted by the appropriate symmetry operations.

5.4. A New Form of Magnetism?

It is interesting to ponder whether the occurrence of magnetic prototypes involving non-interconvertible spin-structure motif pair qualifies as a fundamentally new form of magnetic order relative to the known interconvertible spin-structure motif pair. Recent work[6,39] advocated the idea of branding antiferromagnets with, what is defined here as, non-interconvertible spin-structure motif pair as “a third phase of magnetism” adding to the conventional antiferromagnetism and the ferromagnetism. Historically, antiferromagnetism has been described by Louis Néel[40] as an “antiparallel arrangement of atomic moments”;

the concept was later generalized to describe a specific type of magnetism where "arrangement of atomic moments exactly compensates", including both collinear and noncollinear magnetic ordering. Following this traditional definition, it seems that the magnetic prototypes originating from interconvertible or non-interconvertible spin-structure motif pair (Figure 1d versus Figure 1e) belong to the same underlying antiferromagnetism. Indeed, antiferromagnetic crystals come with many possible symmetries and different point group symmetries come with concomitant variations in material properties. In this respect, it does not seem consistent to distinguish systems with non-interconvertible geometry as a fundamentally different kind of magnetism from Néel antiferromagnetism. The traditional definition—"arrangement of atomic moments that exactly compensates"—already encompasses both.

6. Conclusion

The current work focuses on establishing a structural–motif-based rule, equivalent to the symmetry rule, for selecting the antiferromagnetic compounds with SOC-independent spin splitting effect. Here, we generalized the concept of motif to spin-structure motif–structure motif that carries magnetic moment. We show that the formal symmetry conditions can be interpreted in terms of easy-to-visualize local motifs, such as octahedra or tetrahedra, encompassed with magnetic moments of spin-up and spin-down. Collinear antiferromagnets with such spin-structure motif pair whose components interconvert by neither translation nor spatial inversion will show spin splitting. Such a real-space motif-based approach enables an easy way to identify and design materials having spin splitting without the need for SOC and offers insights on the magnitude and momentum-dependent of the spin splitting. The potential broader impact of the motif-based description has been discussed.

7. Computational Methods

The electronic properties were calculated by the density functional theory (DFT) method[41] implemented in the Vienna Ab initio Simulation Package (VASP). For all the calculations, the Perdew–Burke–Ernzerhof (PBE) exchange-correlation functional[42] was employed with on-site coulomb on 3d orbitals following the simplified rotationally invariant approach introduced by Dudarev et al.[43] A plane-wave basis of up to 500 eV energy cutoff was adopted, a Γ-centered k-mesh for hexagonal crystals, and Monkhorst–Pack[44] k-mesh otherwise for self-consistent charge density. The tetrahedron smearing method was used for insulators or semiconductors and the Gaussian smearing method for metals. The atomic and magnetic structures of the four example compounds for the calculations were taken from X-ray scattering and/or neutron scattering experiments. The different configurations of tilted $LaMnO_3$ models were constructed by a cooperative tilt of the perfect cubic $LaMnO_3$ enforcing the bond length of Mn–O being 2 Å. Atomic positions and lattice vectors were fixed during the DFT self-consistent iterations. The magnetic configurations were simulated in collinear settings without turning on the SOC.

The energy bands were calculated on the conventional high-symmetry k-paths. The spin polarization of the bands was calculated by projecting the eigenstates onto the direction of the common magnetic axis of the collinear antiferromagnetic compound. The strength of the spin splitting for one compound was evaluated as a weighted average in a self-consistent run. The sum of the spin splitting of the occupied bands for each k-point was weighted by the multiplicity of the symmetry-reduced k-points. The averaged spin splitting was then calculated as an average over all k-points of the k sampling for all occupied bands, that was the sum of the spin splitting at different k divided by the number of bands and the number of k-points.

Supporting Information

Supporting Information is available from the Wiley Online Library or from the author.

Acknowledgements

The authors thank Dr. Xiuwen Zhang for stimulating discussions. The work was supported by the National Science Foundation (NSF) DMR-CMMT Grant No. DMR-2113922 that supported the formal theory development of this work. The electronic structure calculations of this work were supported by the U.S. Department of Energy , Office of Science, Basic Energy Sciences, Materials Sciences and Engineering Division under Grant No. DE-SC0010467. This work used resources from the National Energy Research Scientific Computing Center, which was supported by the Office of Science of the U.S. Department of Energy.

Conflict of Interest

The authors declare no conflict of interest.

Data Availability Statement

The density functional theory results that support the findings of this study are openly available in FigShare at https://doi.org/10.6084/m9.figshare.23524584.v2.

Keywords

collinear antiferromagnets, momentum-dependent spin splitting, spin-structure motifs

Received: December 20, 2022
Revised: April 5, 2023
Published online: June 25, 2023

[1] E. Rashba, V. Sheka, *Fiz. Tverd. Tela, Collected Papers (Leningrad)* **1959**, *2*, 62.
[2] G. Dresselhaus, *Phys. Rev.* **1955**, *100*, 580.
[3] S. I. Pekar, E. I. Rashba, *Zh. Eksperim. i Teor. Fiz.* **1964**, 47.
[4] a) L.-D. Yuan, Z. Wang, J.-W. Luo, E. I. Rashba, A. Zunger, *Phys. Rev. B* **2020**, *102*, 014422; b) L.-D. Yuan, Z. Wang, J.-W. Luo, A. Zunger, *Phys. Rev. Mater.* **2021**, *5*, 014409.
[5] a) W. F. Brinkman, R. J. Elliott, R. E. Peierls, *Proc. R. Soc. London, Ser. A* **1966**, *294*, 343; b) D. B. Litvin, W. Opechowski, *Physica* **1974**, *76*, 538; c) D. Litvin, *Acta Crystallogr. A* **1977**, *33*, 279.

[6] L. Šmejkal, J. Sinova, T. Jungwirth, *Phys. Rev. X* **2022**, *12*, 031042.
[7] a) S. Hayami, Y. Yanagi, H. Kusunose, *J. Phys. Soc. Jpn.* **2019**, *88*, 123702; b) S. Hayami, Y. Yanagi, H. Kusunose, *Phys. Rev. B* **2020**, *102*, 144441; c) S. Hayami, Y. Yanagi, H. Kusunose, *Phys. Rev. B* **2020**, *101*, 220403.
[8] a) H. Bai, L. Han, X. Y. Feng, Y. J. Zhou, R. X. Su, Q. Wang, L. Y. Liao, W. X. Zhu, X. Z. Chen, F. Pan, X. L. Fan, C. Song, *Phys. Rev. Lett.* **2022**, *128*, 197202; b) A. Bose, N. J. Schreiber, R. Jain, D.-F. Shao, H. P. Nair, J. Sun, X. S. Zhang, D. A. Muller, E. Y. Tsymbal, D. G. Schlom, D. C. Ralph, *Nat. Electron.* **2022**, *5*, 267; c) S. Karube, T. Tanaka, D. Sugawara, N. Kadoguchi, M. Kohda, J. Nitta, *Phys. Rev. Lett.* **2022**, *129*, 137201.
[9] a) P. Villars, K. Cenzual, J. Daams, Y. Chen, S. Iwata, *J. Alloys Compd.* **2004**, *367*, 167; b) D. Waroquiers, X. Gonze, G.-M. Rignanese, C. Welker-Nieuwoudt, F. Rosowski, M. Göbel, S. Schenk, P. Degelmann, R. André, R. Glaum, G. Hautier, *Chem. Mater.* **2017**, *29*, 8346; c) R. M. Hartshorn, E. Hey-Hawkins, R. Kalio, G. J. Leigh, *Pure Appl. Chem.* **2007**, *79*, 1779; d) J. Lima-de-Faria, E. Hellner, F. Liebau, E. Makovicky, E. Parthe, *Acta Crystallogr. A* **1990**, *46*, 1.
[10] a) C. Ederer, N. A. Spaldin, *Phys. Rev. B* **2007**, *76*, 214404; b) N. A. Spaldin, M. Fechner, E. Bousquet, A. Balatsky, L. Nordström, *Phys. Rev. B* **2013**, *88*, 094429; c) B. B. Van Aken, J.-P. Rivera, H. Schmid, M. Fiebig, *Nature* **2007**, *449*, 702.
[11] S. Bhowal, N. A. Spaldin, arXiv:2212.03756, **2022**.
[12] a) L.-D. Yuan, Z. Wang, J.-W. Luo, A. Zunger, *Phys. Rev. B* **2021**, *103*, 224410; b) L. Šmejkal, R. González-Hernández, T. Jungwirth, J. Sinova, *Sci. Adv.* **2020**, *6*, eaaz8809; c) K. Samanta, M. Ležaić, M. Merte, F. Freimuth, S. Blügel, Y. Mokrousov, *J. Appl. Phys.* **2020**, *127*, 213904.
[13] a) H. Heesch, *Z. Kristallogr. – Cryst. Mater.* **1930**, *73*, 325; b) B. Tavger, V. Zaitsev, *Soviet Phys. JETP* **1956**, *3*, 430; c) A. Zamorzaev, *Kristallografiya* **1957**, *2*, 15; Sov. Phys. Crystallogr. 1957, 2, 10 [English tranlation]; d) L. D. Landau, J. S. Bell, M. J. Kearsley, L. P. Pitaevskii, E. M. Lifshitz, J. B. Sykes, *Electrodynamics of Continuous Media*,2n Ed., Course Theoretical Physics, Vol. *8*, Butterworth-Heinemann, Oxford, UK **1984**; e) C. Bradley, A. Cracknell, *The Mathematical Theory of Symmetry in Solids: Representation Theory for Point Groups and Space Groups*, Oxford University Press, New York, **2010**; f) D. B. Litvin, *Magnetic Group Tables: 1–, 2– and 3–Dimensional Magnetic Subperiodic Groups and Magnetic Space Groups, International Union of Crystallography*, Chester, UK, **2013**.
[14] S. V. Gallego, J. M. Perez-Mato, L. Elcoro, E. S. Tasci, R. M. Hanson, K. Momma, M. I. Aroyo, G. Madariaga, *J. Appl. Crystallogr.* **2016**, *49*, 1750.
[15] F. A. K. Aurenhammer, R. Klein, D. T. Lee, *Voronoi Diagrams and Delaunay Triangulations, World Scientific, Singapore, 2015, p. 225.*
[16] S. P. Ong, W. D. Richards, A. Jain, G. Hautier, M. Kocher, S. Cholia, D. Gunter, V. L. Chevrier, K. A. Persson, G. Ceder, *Comput. Mater. Sci.* **2013**, *68*, 314.
[17] a) P. Wadley, V. Hills, M. R. Shahedkhah, K. W. Edmonds, R. P. Campion, V. Novák, B. Ouladdiaf, D. Khalyavin, S. Langridge, V. Saidl, P. Nemec, A. W. Rushforth, B. L. Gallagher, S. S. Dhesi, F. Maccherozzi, J. Železný, T. Jungwirth, *Sci. Rep.* **2015**, *5*, 17079; b) L. Šmejkal, J. Železný, J. Sinova, T. Jungwirth, *Phys. Rev. Lett.* **2017**, *118*, 106402.
[18] M. K. Wilkinson, J. W. Cable, E. O. Wollan, W. C. Koehler, *Phys. Rev.* **1959**, *113*, 497.
[19] A. A. Belik, S. Iikubo, K. Kodama, N. Igawa, S.-i. Shamoto, S. Niitaka, M. Azuma, Y. Shimakawa, M. Takano, F. Izumi, E. Takayama-Muromachi, *Chem. Mater.* **2006**, *18*, 798.
[20] K. Yamauchi, P. Barone, S. Picozzi, *Phys. Rev. B* **2019**, *100*, 245115.
[21] P. J. Brown, J. B. Forsyth, *J. Phys. C: Solid State Phys.* **1981**, *14*, 5171.
[22] K.-H. Ahn, A. Hariki, K.-W. Lee, J. Kuneš, *Phys. Rev. B* **2019**, *99*, 184432.
[23] Y. Guo, H. Liu, O. Janson, I. C. Fulga, J. van den Brink, J. I. Facio, *Mater. Today Phys.* **2023**, *32*, 100991.
[24] G. Venturini, R. Welter, E. Ressouche, B. Malaman, *J. Alloys Compd.* **1994**, *210*, 213.
[25] A. Glazer, *Acta Crystallogr.* **1972**, *28*, 3384.
[26] S. Quezel-Ambrunaz, *Bull. Mineral.* **1968**, *91*, 339.
[27] A. Muñoz, J. A. Alonso, M. J. Martínez-Lope, J. L. García-Muñoz, M. T. Fernández-Díaz, *J. Phys.: Condens. Matter* **2000**, *12*, 1361.
[28] a) A. T. Zayak, X. Huang, J. B. Neaton, K. M. Rabe, *Phys. Rev. B* **2006**, *74*, 094104; b) J. M. Rondinelli, N. A. Spaldin, *Phys. Rev. B* **2010**, *82*, 113402.
[29] D. Kan, R. Aso, H. Kurata, Y. Shimakawa, *APL Mater.* **2015**, *3*, 062302.
[30] A. Herklotz, A. T. Wong, T. Meyer, M. D. Biegalski, H. N. Lee, T. Z. Ward, *Sci. Rep.* **2016**, *6*, 26491.
[31] A. Virtue, X. Zhou, B. Wilfong, J. W. Lynn, K. Taddei, P. Zavalij, L. Wang, E. E. Rodriguez, *Phys. Rev. Mater.* **2019**, *3*, 044411.
[32] H. Peng, P. F. Ndione, D. S. Ginley, A. Zakutayev, S. Lany, *Phys. Rev. X* **2015**, *5*, 021016.
[33] a) P. Y. Yu, M. Cardona, *Fundamentals of Semiconductors: Physics and Materials Properties*, Springer, Berlin, Germany, **2005**; b) W. A. Harrison, *Electronic Structure and the Properties of Solids: The Physics of the Chemical Bond, Courier Corporation* **2012**.
[34] a) A. Chandrasekaran, D. Kamal, R. Batra, C. Kim, L. Chen, R. Ramprasad, *npj Computational Materials* **2019**, *5*, 22; b) H. R. Banjade, S. Hauri, S. Zhang, F. Ricci, W. Gong, G. Hautier, S. Vucetic, Q. Yan, *Sci. Adv. 7*, eabf1754.
[35] a) J. Daams, P. Villars, in *Proc. Second Int. Conf. on Intelligent Processing and Manufacturing of Materials. IPMM'99 (Cat. No.99EX296)*, IEEE, Piscataway, NJ, USA **1999**, pp. 1339–1360; b) J. L. C. Daams, J. H. N. van Vucht, P. Villars, *J. Alloys Compd.* **1992**, *182*, 1; c) J. L. C. Daams, P. Villars, *J. Alloys Compd.* **1994**, *215*, 1; d) J. L. C. Daams, P. Villars, *J. Alloys Compd.* **1997**, *252*, 110; e) P. Villars, J. L. C. Daams, *J. Alloys Compd.* **1993**, *197*, 177.
[36] N. A. Hill, K. M. Rabe, *Phys. Rev. B* **1999**, *59*, 8759.
[37] F. Sugawara, S. Iiida, Y. Syono, S.-i. Akimoto, *J. Phys. Soc. Jpn.* **1968**, *25*, 1553.
[38] R. A. de Groot, F. M. Mueller, P. G. v. Engen, K. H. J. Buschow, *Phys. Rev. Lett.* **1983**, *50*, 2024.
[39] I. Mazin, *Phys. Rev. X* **2022**, *12*, 040002.
[40] a) L. Néel, *J. Phys. Radium* **1932**, *3*, 160; b) L. Néel, *Proc. Phys. Soc., London, Sect. A* **1952**, *65*, 869.
[41] a) W. Kohn, A. D. Becke, R. G. Parr, *J. Phys. Chem.* **1996**, *100*, 12974; b) P. Hohenberg, W. Kohn, *Phys. Rev.* **1964**, *136*, B864; c) W. Kohn, L. J. Sham, *Phys. Rev.* **1965**, *140*, A1133.
[42] a) P. E. Blöchl, *Phys. Rev. B* **1994**, *50*, 17953; b) G. Kresse, D. Joubert, *Phys. Rev. B* **1999**, *59*, 1758; c) J. P. Perdew, K. Burke, M. Ernzerhof, *Phys. Rev. Lett.* **1996**, *77*, 3865.
[43] S. L. Dudarev, G. A. Botton, S. Y. Savrasov, C. J. Humphreys, A. P. Sutton, *Phys. Rev. B* **1998**, *57*, 1505.
[44] H. J. Monkhorst, J. D. Pack, *Phys. Rev. B* **1976**, *13*, 5188.